Deliverable number: D1.2.

DACOMAT - Damage Controlled Composite Materials

Cohesive zone model for mode I and mode II delamination

Reidar Kvale Joki

The DACOMAT project has received funding from the European Union's Horizon 2020 research and innovation programme under GA No. 761072

Deliverable details

Document name: Cohesive zone model for mode I and mode II delamination

Responsible partner: FIRECO

Work package: WP1 – Concept Modelling

Task: Task 1.2: Cohesive zone modelling

Due date: 31.12.2019

Delivery date: 31.12.2019

Dissemination level	
x	PU = Public
	CO = Confidential, only for members of the consortium (including the EC)
	Classified, information as referred to in Commission Decision 2001/844/EC.
Deliverable type	
x	R: Document, report (excluding the periodic and final reports)
	DEM: Demonstrator, pilot, prototype, plan designs
	DEC: Websites, patents filing, press & media actions, videos, etc.
	OTHER: Software, technical diagram, etc.

The DACOMAT project has received funding from the European Union's Horizon 2020 research and innovation program under GA No. 761072

Popular science summary

Cohesive elements are highly instrumental for modelling delamination in fibre-reinforced polymer composites laminates. As such, the cohesive laws that govern these elements must be derived from thorough mechanical experiments. This report details the physical mechanisms that affect fracture resistance and crack growth, namely: crack tip opening and fibre bridging. In turn, it presents two key challenges facing current fracture toughness test methods. First, there exists a small yet significant incongruence between the actual crack tip position within a specimen and the position conventionally observed at the surface. This discrepancy is due to the presence of anticlastic bending, which is influenced by a given laminate's elastic properties and the selected specimen geometry. Second, current test methods determine the fracture energy with respect to the crack end opening evolution. The opening evolution at the crack front is affected by the presence of fibre bridging and therefore evolve at a slightly different opening mode than that observed at the crack end. The energy dissipated during the development of a crack tip is significantly affected by the opening mode. The separation of steady state fracture resistance into crack tip and fibre bridging contributions is therefore difficult. An iterative characterization procedure is instead proposed in this report to overcome both of these challenges.

Contents

The DACOMAT project has received funding from the European Union's Horizon 2020 research and innovation program under GA No. 761072

1. Introduction

This report presents the results of the cohesive zone modelling work that was performed in Task 1.2 of Work Package 1 (WP1). The work objective for this task is given below.

Task 1.2: Cohesive zone modelling Use existing numerical methods for mode I, mixed mode and mode II delamination with detailed R curves to investigate how the cohesive law can be designed to promote multiple crack initiation, and how this can lead to crack arrest. Establish a framework for obtaining crack initiation and steady state fracture resistance as functions of delamination mode from cohesive law for use in fatigue analysis. • Subtask 1.2.1: A simple and robust cohesive model clearly distinguishing between tractions associated to crack-tip deformations and fibre bridging will be established and demonstrated to reproduce fracture resistance of FRP laminates. • Subtask 1.2.2: The shape of the cohesive law gives a good representation of the relation between threshold tractions for initiation of delamination and tractions related to fibre bridging. This relation will be investigated in this subtask with the aim of identifying the characteristics of secondary delamination initiation. It is here important to relate the micromechanical relations from task 1.1 to the cohesive law.

The aim of this report is to provide the reader with a general understanding of how to model delamination via Finite Element Modelling (FEM), which model input is required and how to obtain this input from mechanical experiments. The characteristics of crack tip deformations and large-scale bridging, and how these two phenomena affect the cohesive properties of a delaminating FRP laminate are discussed. A description is given on how the micromechanical models presented in DACOMAT deliverable 1.1 *Micromechanical modelling* (D1.1) benefit the characterisation of cohesive zone models. It also serves as a knowledge base for better understanding the challenges that are addressed when seeking to promote secondary, parallel crack fronts described in DACOMAT deliverable 1.3 *Determining the governing factors for promotion of secondary delamination fronts* (D1.3), and when modelling fatigue-driven delamination described in DACOMAT deliverable 1.4 *Fatigue model based on a cohesive law* (D1.4).

This report is organized as follows. Section 2 introduces the topic of delamination and gives an overview of the terminology used throughout this report. Thereafter, a theoretical basis for cohesive zone modelling is given in section 3. The challenge of charactering the modelling parameters for cohesive zone models are addressed in section 4. The findings made during the first two years of Dacomat are presented in section 5. Finally, some concluding remarks and recommendations are provided in section 6.

2. Delamination fracture mechanics

Multiaxial laminates are susceptible to intra-laminar cracking due to their layered anisotropic nature. The initiation and progression of these intra-laminar cracks are normally referred to as delamination. The initiation of delamination is partly similar to the development of intra-laminar matrix cracking associated with first ply failure. Matrix cracking takes the general physical appearance of a set of numerous cracks spread out over a homogeneously orthotropic volume and can be seen as smeared out reduction of active area for stress transfer or as a degradation of stiffness. Such developments are well described in terms of continuum damage mechanics. Delamination, on the other hand, represents a distinct and extensive strain discontinuity. It is therefore best described in terms of fracture mechanics where a traction-separation law can be used to define the properties of crack initiation and propagation.

FRP laminates are often introduced in structural applications as primary structural members in the form of panels or beams, which are both susceptible to delamination. The fracture energy dissipated as a delamination crack propagates is usually attributed to the work carried out by some external driving force. Some sort of bending is often involved, however delamination can also be caused by other mechanisms, namely 1) local buckling caused by in-plane compression, and 2) shear-induced delamination in test coupons with ±45˚ ply orientations with respect to the loading direction. These two examples and the more general case of bending cover the three distinct modes of delamination (Figure 1). Mode I represent a normal opening mode commonly referred to as peeling. Mode II is the type of sliding shearing that is seen in laminates subjected to bending. Mode III is a second shearing mode with a rotational component about the through-thickness direction of the laminate. Delaminations addressed in this report will be limited to modes I and II.

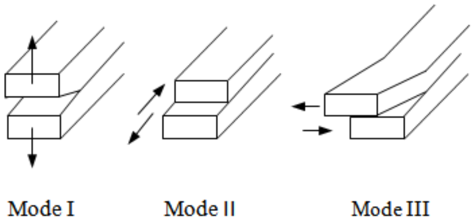

Figure 1. Three modes of delamination.

3. Cohesive zone modelling

Cohesive zone modelling is a tool to evaluate the loads transferred across the interface between two fracturing surfaces as they separate. The characteristics of the interface is described in terms of traction and separation. The properties of an interface that is susceptible to delamination can be defined in terms of a cohesive law. The cohesive law prescribes the cohesive stiffness and the maximum tractions that can be transferred between the fracturing surfaces at a given magnitude of separation. The cohesive stiffness is the rate of cohesive traction to opening separation. The method was first introduced in a finite element analysis (FEA) by Geubelle and Baylor in 1998 [1], and is now available in most commercial FE codes.

3.1. FE modelling of delamination

There are numerous reasons for wanting to model delamination via FEM. For instance, modelling the evolution of delamination can increase the understanding of delamination initiation and propagation. A partly delaminated beam or panel will have significantly lower bending stiffness compared to the respective pristine structure. Including delamination in a nonlinear analysis is therefore crucial for understanding how complex loads are redistributed during failure. Such analysis can include impact modelling, for which delamination is assumed to be a significant contributor to the total damage energy, or fatigue simulations of structural details susceptible to delamination.

Different analyses might have different demands for the FE description of the delamination. For instance, cases, in which load increases continuously up to ultimate failure, do not require a correct unloading description. In contrast, fatigue and impact cases would benefit from capturing the correct unloading behaviour. Nonetheless, there are fundamental aspects of delamination that will be need to be captured by most analyses, namely: are cohesive stiffnesses, maximum cohesive tractions, maximum opening displacements and critical cohesive energies (or critical energy release rates).

The DACOMAT project has received funding from the European Union's Horizon 2020 research and innovation program under GA No. 761072

3.2. Cohesive Law

The cohesive law depends on the laminate constituents (i.e. matrix and fibres) and the fibre volume fraction. As such, it can be considered to be a "material property" for a given laminate. This consideration is however debatable as since the law can vary with both fibre volume fraction and, possibly, with the fibre orientation of adjacent plies.

The cohesive law ought to include the properties listed in sub-section 3.1, namely: cohesive stiffnesses, maximum cohesive tractions, maximum opening displacements and critical cohesive energies. The cohesive law is best described as a surface in the space of the two opening directions (mode I and II) and the cohesive tractions. One surface for each of the two cohesive tractions is needed, with the cohesive traction on one axis and the opening displacements on the other two. As described in the literature, the cohesive law is often illustrated as a bilinear curve with the opening displacement on the horizontal axis and cohesive traction on the vertical. This curve is the simplest curve that will do the job in a FEA. The bilinear shape describes quite comprehensively the aforementioned properties. Starting from zero cohesive traction, σ, and zero opening displacement, δ, the initial line represents the cohesive stiffness, k (Figure 2). The intersection point between the two straight lines represents the maximum cohesive traction, σ_c. In turn, the point at which the curve reconnects with the horizontal axis represents the maximum opening displacement, δ_0. Finally, the critical cohesive energy is represented by the area under the bi-linear curve, G_c.

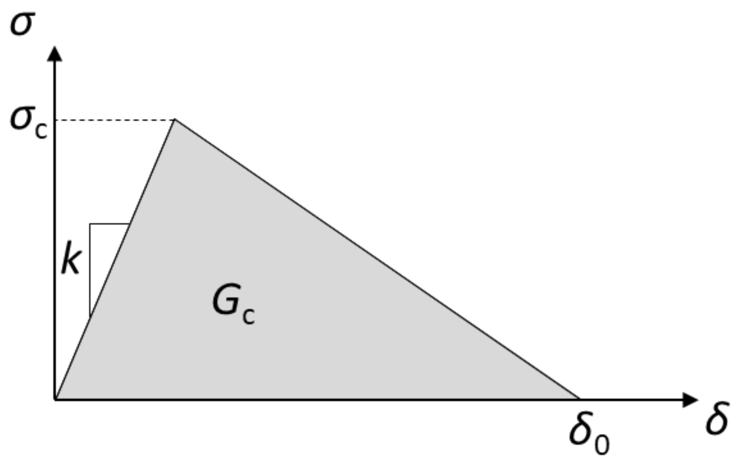

Figure 2. Bi-linear cohesive law.

3.3. Cohesive Elements

The cohesive element is a tool for implementing the cohesive law in an FE model. The cohesive elements will be placed at the interface, where the delamination is expected to propagate. The purpose of the cohesive elements is to ensure that the elements of the elastic bodies adjacent to the fracture interfaces experience the correct boundary tractions during the evolution of delamination. The constitutive relations for cohesive elements are typical the following form,

$$\begin{bmatrix}\sigma_1\\ \sigma_2\\ \sigma_3\end{bmatrix} = \begin{bmatrix}k_1(1-D) & 0 & 0\\ 0 & k_2(1-D) & 0\\ 0 & 0 & k_3(1-D)\end{bmatrix}\begin{bmatrix}\delta_1\\ \delta_2\\ \delta_3\end{bmatrix}, \tag{1}$$

where σ_i, k_i and δ_i are the cohesive tractions, stiffnesses and opening displacements, respectively. The parameter D is the damage parameter that is used to prescribe the correct cohesive traction during separation. The numerical subscripts 1, 2 and 3 refer to the orthogonal opening directions. Subscript 1 and 2 conventionally indicate in-plane opening displacements associated with mode II, and subscript 3 indicates normal opening displacements associated with Mode I. There generally are no off-axis relations in the stiffness matrix for cohesive elements, which implies that the opening modes are decoupled.

4. Characterisation of cohesive properties

When attempting to characterize the cohesive properties of FRP laminates it is useful to take a look at the fracture resistance curve, hereafter referred to as the R-curve. The R-curve is a function of the work that goes into opening a crack with respect to the opening displacement of the crack-end.

The R-curve is a useful tool to illustrative the different types of fracture mechanisms (Figure 3). In a brittle material for instance, the work carried out by external forces will be absorbed in the form of elastic energy until a critical level is reached, beyond which crack initiation and propagation occurs. The crack propagation speed increases as the elastic energy supplied by external forces increases, and the crack growth pauses as the elastic energy decreases below the critical level. The R-curve of such brittle materials is bi-linear (Figure 3 a): first an increase in fracture energy or resistance without any opening displacement until the critical energy level is reached at which point the second linear path is followed by an increase in opening displacement without any change in fracture resistance. This type of R-curve is representative of crack evolutions that are covered by linear elastic fracture mechanics (LEFM).

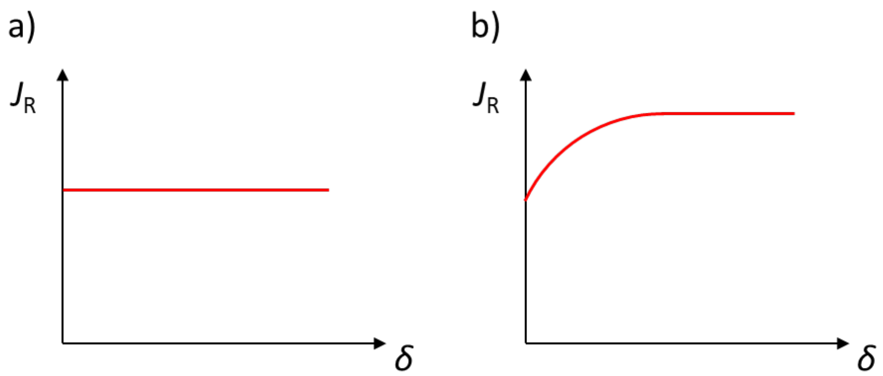

Figure 3. R-curves with crack opening displacement on horizontal axis and fracture resistance at the vertical axis. With a) a flat R-curve typical for brittle fractures and b) a rising R-curve typical for ductile fractures.

For crack propagation in ductile materials, the initial opening of the crack represents plastic deformations around the crack tip. These plastic deformations will activate a larger region of the bulk material that will contribute to resisting further crack tip opening. The R-curve for ductile fracture is marked by an increase in fracture resistance during crack tip opening (Figure 3 b). It is typically said that ductile materials display a “rising” R-curve whereas brittle materials display a “flat” R-curve.

Delaminating FRP laminates can display R-curves that are somewhat similar to the rising R-curves of ductile materials. Only in this case the increase in fracture resistance during crack propagation is attributed to fibres bridging between the fracturing surfaces in the wake of the crack tip. These bridging fibres can significantly contribute to the total fracture resistance of the laminate. It should be noted that the magnitude of the crack opening where fibre bridging operates in the wake of the crack tip is of a different scale to that of the crack tip deformations. Laminates that display large scale bridging can have a rising R-curve over crack end opening displacements up to several centimetres. In comparison, the crack tip deformations are thought to be limited to roughly 100 micrometres.

To complicate the matter, the crack tip can display both brittle and ductile behaviour. In mode I delamination, the crack tip is thought to be brittle, whereas mode II promotes a more ductile crack tip behaviour. The difference in stress triaxiality between the two modes supports the notion that mode I should display more brittle behaviour than mode II. The same reasoning can explain why adhesive bonds should be loaded in shear rather than peel. The polymers generally used in FRP laminates have similar properties to those of commonly used adhesives. Critical energy release rate typically reported in the region of 150-300 J/m^2 for mode I and 900-1200 J/m^2 for mode II (without fibre bridging). The range difference is explained by the presence of plastic deformations in mode II.

The bilinear cohesive law is, as mentioned above, often used for illustrative purposes. Several studies have investigated the possibility of determining the actual shape of the cohesive law [2] [3] [4] [5]. The bilinear function is not only used for illustrative purposes. It is actually one of the most commonly used shape for cohesive laws describing delamination, though other functions have also been used. Figure 4 illustrates some commonly used shapes. The use of the bilinear cohesive law is described by Iannucci [6], Dantuluri et al. [7], Xie et al. [8] Bouhala et al. [9] and Camanho et al. [10] - among others. Tvergaard [11] used a polynomial function to model fibre matrix debonding. Polynomial functions have also been described by El-Sayed and Sridharan [12], and Blackman [13]. The exponential function is described by Xu and Needleman [14] and later by van den Bosh et al. [15] and Wagner and Balzani [16]. Finally, the trapezoidal function was proposed by Tvergaard and Hutchinson [17], and later used by Yang and Cox [18] and Østergaard [19] - among others.

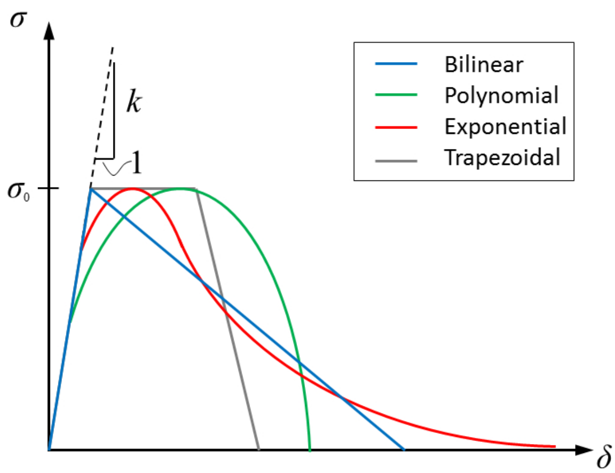

Figure 4. Various suggested cohesive law functions.

4.1. Experimental testing

Several testing standards currently exist for characterising the interlaminar properties of FRP laminates. Mode I characteristics have been studied by loading double cantilever beam (DCB) specimens with wedging forces (traction normal to the crack path). The ASTM D5528 test standard describes how the DCB test ought to be carried out to determine the interlaminar fracture toughness in mode I. Mode II characteristics has been studied by using the same type of DCB specimens loaded instead in three-point-bending. The ASTM D9505 test standard describes how to determine the interlaminar fracture toughness in mode II. The mode II test is commonly referred to as end-notch flexure (ENF). Modes I and II have different characteristics and mixed mode I/II needs to be investigated to see how a delamination behaves when the opening mode is a combination of the two. Mixed mode delamination can be investigated using the ASTM D6671 test standard. It is called mixed mode bending and combines three-point-bending with a wedging force.

One of the main disadvantages with the standardised delamination tests is the challenge of recording the location of the crack tip during the progression of delamination. The work carried out by the external forces depends on the stiffness of the DCB sample, which in turn changes as the crack propagates. These standardised tests are designed for determining the critical energy release rate under the premises of linear-elastic fracture mechanics (small-scale fracture process zone). The fibre bridging will provide a large-scale fracture process zone and thus alter the beams curvature along a significant length of the beam. The presence of large-scale bridging therefore makes the method invalid. For this reason, ASTM D5528 test standard recommends that the orientation of the two plies adjacent to the pre-cracked interface be rotated by a few degrees in opposite directions to reduce the amount of bridging fibres. Such a recommendation does not offer an acceptable way forward for the DACOMAT Project, where the aim is to evaluate the effects of fibre bridging and increase its occurrence to improve fracture toughness.

Olsson and Stigh [5] demonstrated that by measuring the rotations at the end of DCB specimens it would be possible to calculate the interlaminar fracture toughness for mode I without having to record the position of the crack tip. Loading the beam-ends with moments rather than wedging forces will directly produce the same outcome. Equal moments applied to the beam ends will promote mode II delamination. In turn, moments with the same magnitude but opposing directions will promote mode I delamination, and unequal moments will promote mixed mode I/II delamination. The use of bending moments to characterise interlaminar fracture resistance is well described by Sørensen el. al. [4]. Over the past decade, this methodology has gained interest in both the research and industrial FRP communities. The capability of obtaining the fracture resistance in the presence of large-scale bridging makes it especially favourable over current standardized methods. This method is ideally suited to meet the aims of the DACOMAT Project, i.e. to improve fracture toughness and resistance by increasing the amount of fibre bridging. The next section delivers a brief introduction to the methodology behind this approach.

4.2. The *J*-integral approach

The path independent *J*-integral [20] has been adopted to determine the cohesive laws from experiments for plane-stress cases [4] [3] [2] [2] [21]. This approach has made it possible to experimentally determine the shape of the cohesive law. For large-scale bridging (LSB) problems, the *J*-integral of the traditional DCB specimen loaded with wedge forces can be determined by measuring the rotations where the forces are applied [5] [22], which will require additional instrumentation compared to the LEFM test. There is no need, however, to monitor the crack tip position during the test, which is quite challenging. As mentioned in the previous sub-section, the need to measure rotations can be avoided by applying pure bending moments to the test specimens instead of forces [2] [23]. For a DCB specimen loaded with pure bending moments, the *J*-integral is given in closed analytical form, independent of crack length and valid for LSB problems.

The path independent *J*-integral was first applied to crack problems by Rice [20] and can be used to calculate the fracture resistance, J_R. Evaluating the *J*-integral along the external boundaries of the DCB specimen in Figure 5 c) and assuming plane stress results in the following equation [2],

$$J_{R,ext} = \frac{21(M_1^2 + M_2^2) - 6M_1M_2}{4B^2H^3E_{11}} \qquad |M_1| < M_2, \tag{2}$$

where M_1 and M_2 are the moments applied to the beam ends, *B* and *H* are the beam width and height, respectively and E_{11} is the Young's modulus in the x_1-direction.

Evaluating the *J*-integral along the edge of the Fracture Process Zone (FPZ) in Figure 5 a) results in the following equation [2]

$$J_{R,FPZ} = \int_0^{\delta_n^*} \sigma_n(\delta_n, \delta_t)\, d\delta_n + \int_0^{\delta_t^*} \sigma_t(\delta_n, \delta_t)\, d\delta_t, \tag{3}$$

where σ_n and σ_t are the local normal and tangential tractions (both functions of the local normal and tangential separations, δ_n and δ_t)[1], and δ^*_n and δ^*_t are the openings at the end of the failure process zone (FPZ). The cohesive law in Equation (3) represents the entire fracture process including the crack tip separation. The energy associated with the crack tip (*J*-tip) from Figure 5 a) is embedded in the two integrals via the cohesive laws (refer to Figure 5 b). The integrals in equation (3) can be understood as the work per unit area of the normal and tangential tractions at the end of the active cohesive zone.

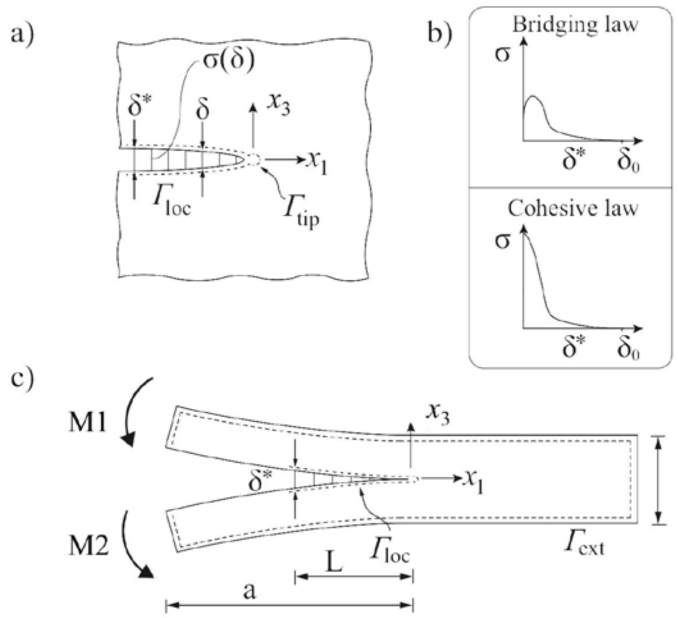

Figure 5. a) Local integration path along fracture process zone, b) bridging law and cohesive law, c) external and local integration paths.

[1] The cohesive tractions prescribed by the cohesive law depend on both normal and tangential opening displacements. This is not a contradiction to that stated in Equation (1). Equation (1) relate to the constitutive relations of a cohesive element. The tractions in Equations (3) governs the value of the damage parameter D in Equation (1).

The DACOMAT project has received funding from the European Union's Horizon 2020 research and innovation program under GA No. 761072

Due to path-independence, $J_{R,ext} = J_{R,FPZ}$ [20]. A large portion of the fracture energy, $J_{R,FPZ}$, dissipated from crack initiation to total separation is caused by crack tip deformations. This portion of the fracture energy is normally referred to as J_0 and is characterised by small opening displacements and high tractions. When $J_{R,ext} > J_0$, the dissipated fracture energy is assumed to be caused by fibre bridging. This part of the fracture process is characterised by larger opening displacements and significantly lower tractions. With increasing $J_{R,ext}$, the length of the active cohesive zone, L, and the end-opening, $\delta^* = \sqrt{(\delta_n^*)^2 + (\delta_t^*)^2}$, increase as the crack extends. When δ^* reaches a critical value, δ_0, the fracture surfaces are completely separated at the end of the FPZ. The FPZ is then fully developed, and the fracture resistance attains a constant value referred to as the steady-state fracture resistance, J_{ss}. The values of J_{ss}, δ_0 and J_0 depend on the opening mode.

By conducting several delamination experiments with moment combinations ranging from pure mode I to mode II while monitoring the crack end opening displacements, a surface describing the fracture resistance as a function of normal and tangential opening can be established as $J_{R,ext}(\delta_n^*, \delta_t^*)$. The cohesive laws for normal and tangential cohesive tractions can then be determined by partial differentiation [2]:

$$\sigma_n(\delta_n^*, \delta_t^*) = \frac{\partial J_{R,ext}(\delta_n^*, \delta_t^*)}{\partial \delta_n^*} \qquad \sigma_t(\delta_n^*, \delta_t^*) = \frac{\partial J_{R,ext}(\delta_n^*, \delta_t^*)}{\partial \delta_t^*} \tag{4}$$

Equation (4) can be understood as giving the values of the normal and tangential tractions at the end of the cohesive zone. Assuming that the cohesive laws are the same at any location within the cohesive zone, the traction separation laws obtained using equation (4) are thus representative for the entire cohesive zone.

The cohesive law can either include both crack tip behaviour and fibre bridging, or simply fibre bridging tractions. The first case is what it is normally meant when referring to a cohesive law and the latter can, for the sake of distinguishing the two, be called a bridging law (Figure 5 b). Before conducting partial differentiation of the fracture resistance, the experimental results require some processing. A challenge with fitting functions to the experimental results is that the experimental R-curves include the behaviour of the crack tip deformation and the fibre bridging. The evolution of the crack tip deformations is associated with small opening displacements and large tractions, whereas the fibre bridging is associated with significantly larger opening displacements and significantly smaller tractions. The crack tip deformations are part of the fracture resistance as previously mentioned, referred to as J_0 and the maximum fracture resistance as, J_{SS}. By subtracting J_0 from J_{SS}, one could argue that only the fracture resistance associated with fibre bridging remains (Figure 6).

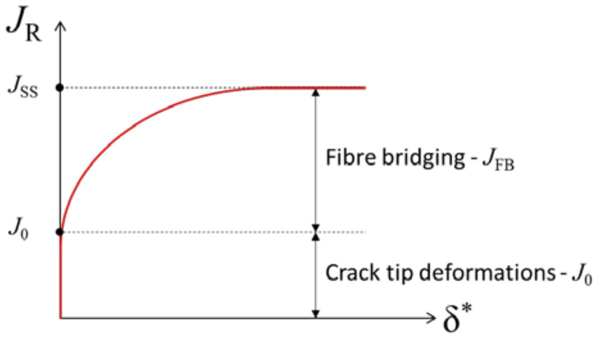

Figure 6. A schematic representation of the relation between crack tip and fibre bridging contributions to the fracture resistance.

The DACOMAT project has received funding from the European Union's Horizon 2020 research and innovation program under GA No. 761072

4.3. Anticlastic bending

Joki et al. [24] found that the opening displacements measured at the side of the test specimen were not representative for initiation and early development of mode I dominated delaminations. When a beam is subjected to bending, the Poisson's effect causes bending stress in the transverse direction. This transverse bending stress give rise to what is called anticlastic bending. The effect is small and normally negligible for the overall behaviour of beams in bending. However, this effect is not insignificant for observing the small openings associated with crack tip deformations. A closer examination of the experimental results presented in [24] indicated the presence of compression at the side of the specimens near the initial crack tip prior to crack opening. Figure 7 demonstrates a slight negative displacement before the opening accelerate in the positive direction. The pin position, at which opening displacements are recorded, clearly affects measurement of the initial opening. The specimen CHOA01A-05 curve may therefore be located slightly towards the applied moments side and the specimen CHOA01A-06 curve slightly towards the other side of the initial crack tip.

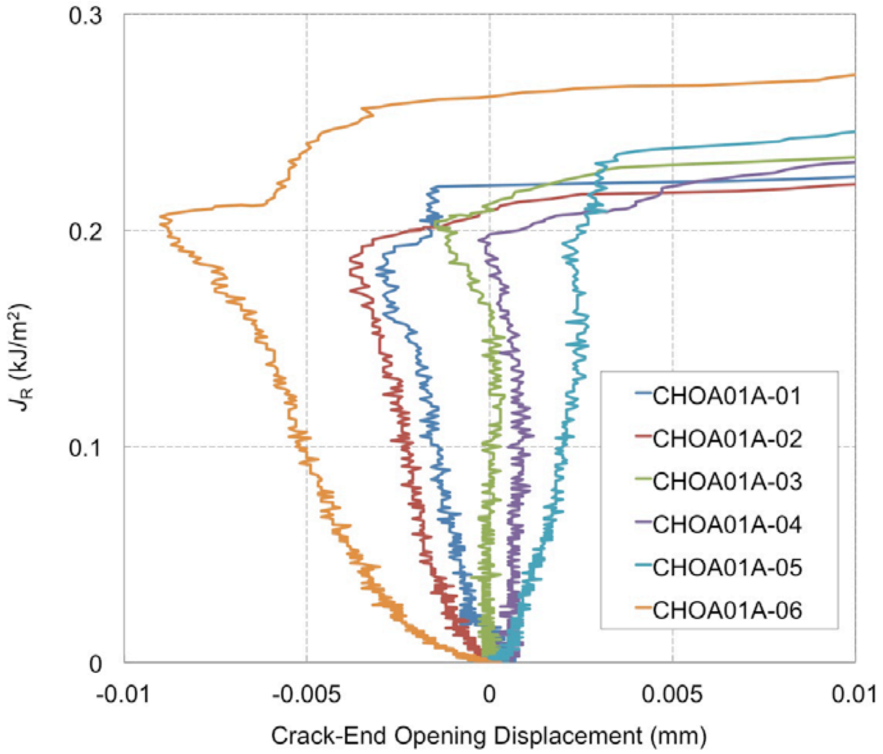

Figure 7. Initial Mode I opening of a DCB sample loaded with bending moments. Opening measured by extensometer clamped to pins drilled into the sides of the beams at the initial crack tip.

The anticlastic bending effect will force the crack tip initiation to open at the mid width of the specimen whilst the edges are pressed together. The opening displacements observed at the side of the specimen will therefore overestimate the portion of the fracture resistance associated with the crack tip. The anticlastic bending effect must therefore be taken into account when determining the cohesive properties from experimental data. Its effect can be demonstrated via a 3D FE model using a bi-linear cohesive law on a high-fidelity representation of a DCB sample.

The DACOMAT project has received funding from the European Union's Horizon 2020 research and innovation program under GA No. 761072

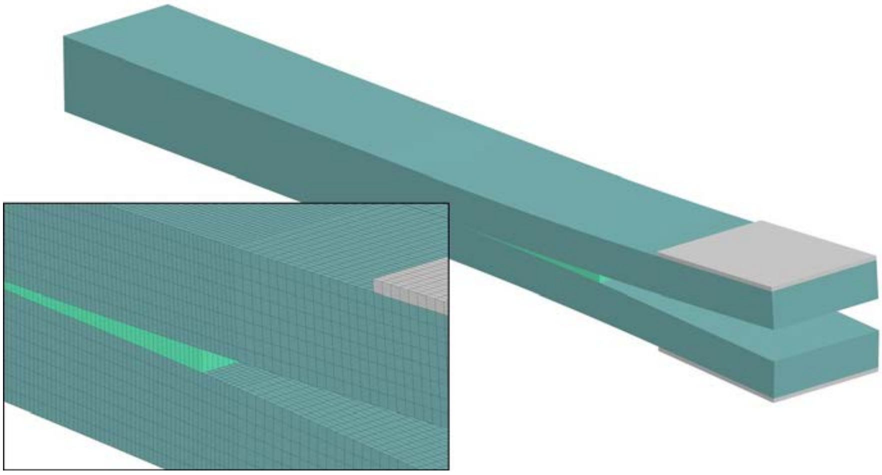

Figure 8. An FE model of a three-dimensional representation of a DCB sample with cohesive elements [24].

A cohesive law can be determined by post processing results from the FE analysis of the beams in Figure 8 using the *J*-integral approach according to Equation (4). The opening deformations are recorded at the same locations used in the mechanical experiments described by Joki et al. [24]. To study the effect of the anticlastic bending, both the Poisson's ratio and the width of the beams were varied. The resulting cohesive laws curves are presented in Figure 9.

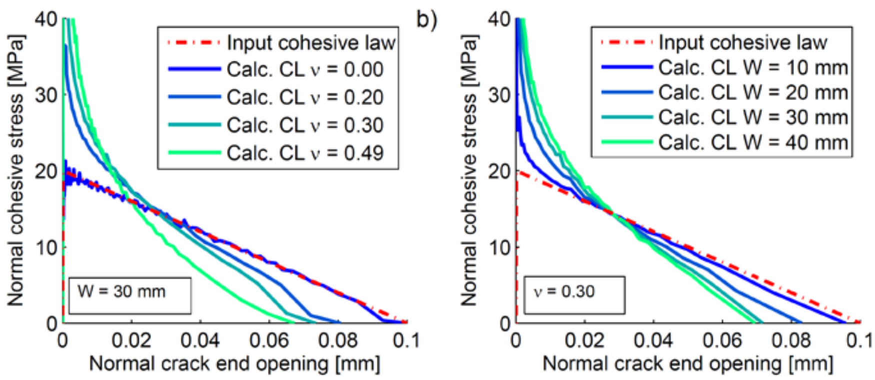

Figure 9. Cohesive laws calculated using the J-integral approach compared to cohesive law used in the FE-model [24].

The results presented in Figure 9 clearly show that there is a discrepancy between cohesive law determined via FEM (using the *J*-integral approach) and the cohesive laws used as input to the analysis. The anticlastic bending is a result of the Poisson's effect and the magnitude of the discrepancy between calculated and input cohesive law should therefore be affected by the Poisson's ratio, as demonstrated in Figure 9 a). The amplitude of the discrepancy in opening at the side surface and mid-width of the specimen will differ based on the width of the specimen. The discrepancy between calculated and input cohesive laws should therefore differ with changing width, as is demonstrated in Figure 9 b).

The consequence of the anticlastic bending effect was overcome by Joki et. al. [24] by using an optimisation scheme where a cohesive law calculated using the *J*-integral approach was used as a starting point. The recorded fracture resistance curve was used as an optimisation goal. The optimised cohesive law was controlled and found capable of predicting the response on the same materials tested in standardised delamination tests. These test specimens differed in geometry compared to those used to calculate and optimise the cohesive law.

The same methodology has been performed on mixed-mode delamination and a manuscript has been submitted and was under peer review at the time this report was written.

5. Cohesive law in the DACOMAT Project

One of the challenges first addressed by the DACOMAT Project team was the separation of crack tip and fibre bridging mechanisms into two distinct cohesive laws based on the assumption illustrated in Figure 6. The initial (vertical) part of the R-curve is found to be caused by crack-tip deformations, while the rising part of the R-curve is caused by fibre bridging. This separation would simplify the fitting operation when creating a surface that is suitable for partial differentiation according to Equation (4). The shape of the cohesive law for the crack tip portion of the R-curve does not seem to be as important as for the fibre bridging portion. The assumption has been that the total energy and the critical tractions are the only significant aspects for the cohesive law describing the crack tip deformations. Differentiation of the vertical incline in the R-curve during the crack tip deformations is awkward since it demands an infinitely high cohesive traction. By separating the two mechanisms into distinct laws the partial differentiation of a fitted surface to the fibre-bridging portion becomes feasible.

A set of R-curves from a series of 5 different moment configurations tested on DCB-samples of the type described in [24] are plotted in Figure 10. The legend in the plot refers to the degree of mode mixity, with mode I = 0˚ and mode II = 90˚. The fracture resistance associated with the crack-tip deformations, J_0, is plotted in Figure 11. Subtracting J_0 from the R-curves in Figure 10 gives the curves plotted in Figure 12. These curves were assumed to describe the fracture resistance contributions from fibre bridging.

The DACOMAT project has received funding from the European Union's Horizon 2020 research and innovation program under GA No. 761072

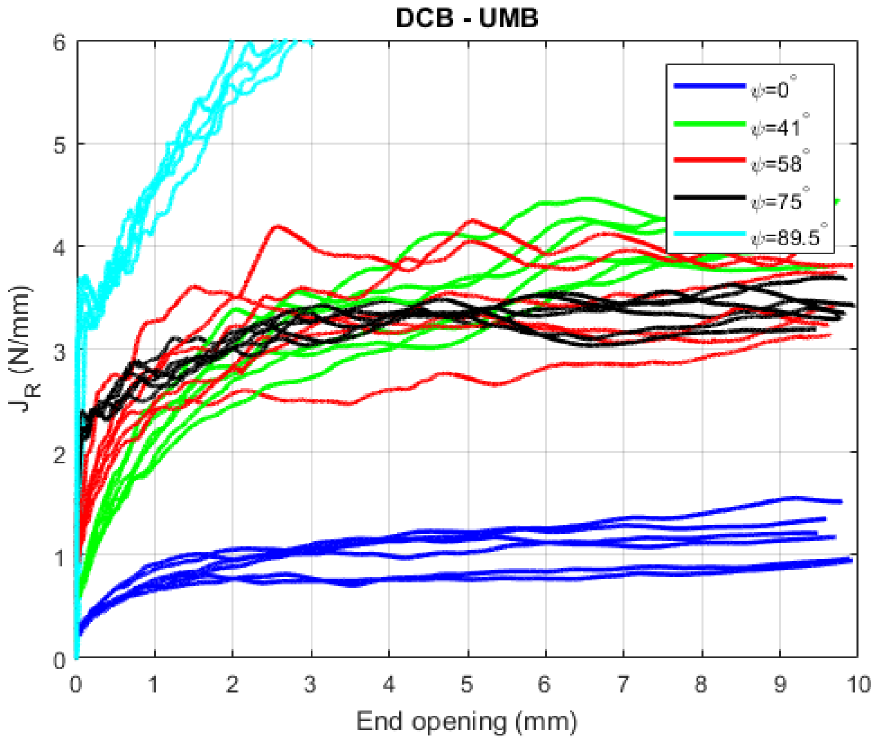

Figure 10. R-curves from five different delamination modes.

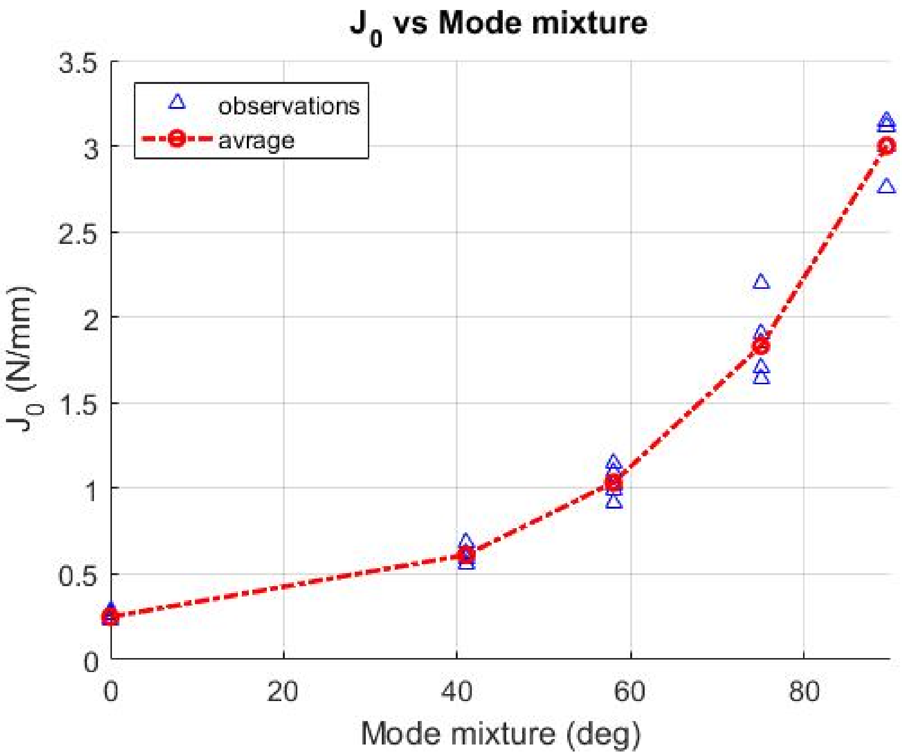

Figure 11. The fracture resistance associated with the crack tip deformations from the R-curves in Figure 10.

The DACOMAT project has received funding from the European Union's Horizon 2020 research and innovation program under GA No. 761072

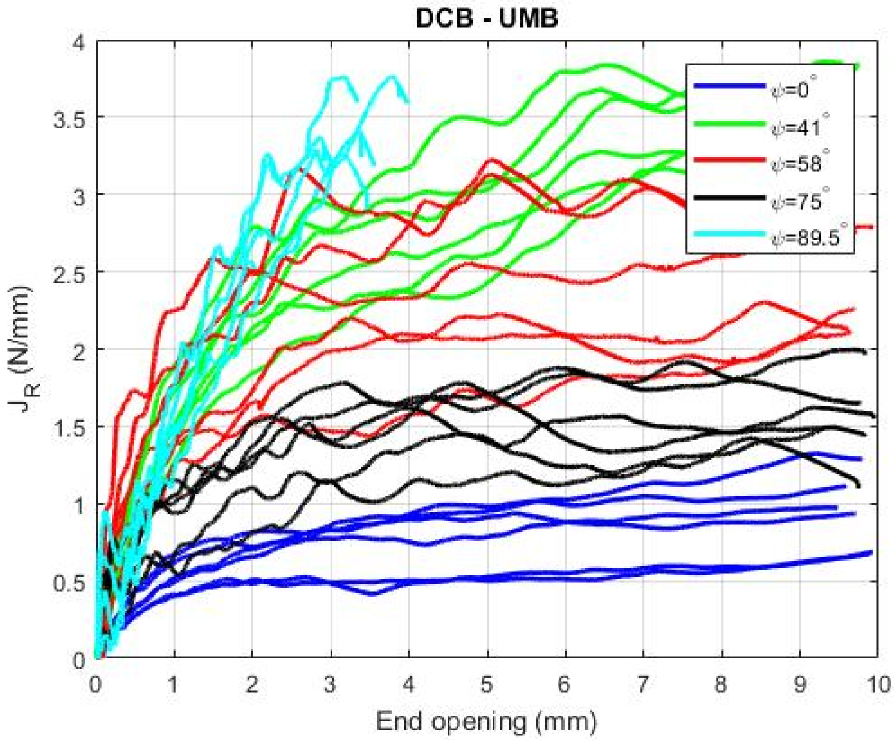

Figure 12. The fracture resistance assumed associated with fibre bridging after J_0 plotted in Figure 11 is subtracted from R-curves in Figure 10.

The process of going from the R-curves in Figure 10 to those in Figure 12 build on the assumption that the crack tip energy is constant as the crack extends and the fracture process zone increase in size. This assumption might not hold up to scrutiny, which is discussed in the next sub-section.

5.1. Opening mode of a crack tip with a wake of fibre bridging

The opening mode of the crack tip is defined by the relative curvature of the two separating beams where they meet at the crack-tip (Figure 13). For the initial crack tip, this curvature is defined by the moments applied to the beam ends. The presence of fibre bridging must clearly affect the curvature of the beams, otherwise there could not be any increase in fracture resistance from fibre bridging. The question then becomes whether the change in curvature preserves the initial rate caused by the moment configuration, or if the delamination mode is changed. To investigate this question, consider a DCB specimen loaded with unequal bending moments that display large scale fibre bridging as illustrated in Figure 13. A schematic illustration of the tractions acting in the failure process zone from bridging fibres in tension is presented in Figure 14, and compression in Figure 15.

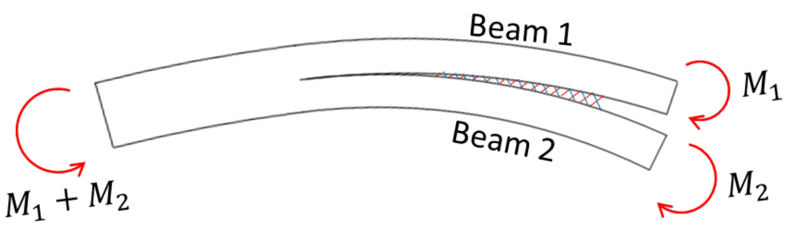

Figure 13. A DCB specimen loaded with unequal bending moments.

The DACOMAT project has received funding from the European Union's Horizon 2020 research and innovation program under GA No. 761072

The question that needs to be answered is whether or not the opening mode at the initial crack tip, ψ_0, is equal to that of the steady-state crack tip, ψ_1. This question can be answered by evaluating the effects of the bridging fibres loaded separately in tension and compression (Figure 14 and Figure 15, respectively).

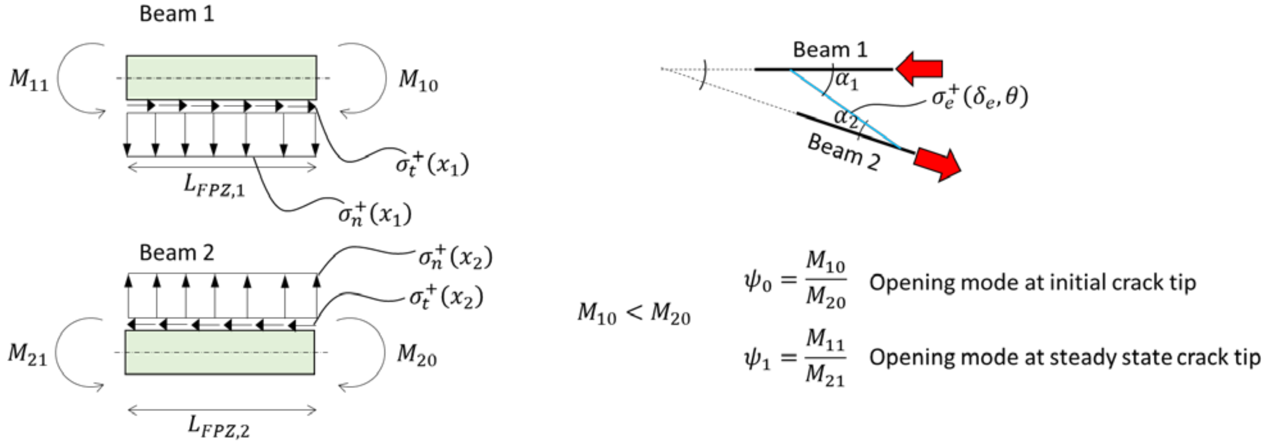

Figure 14. Tractions acting along the fracture process zone due to bridging fibres loaded in tension.

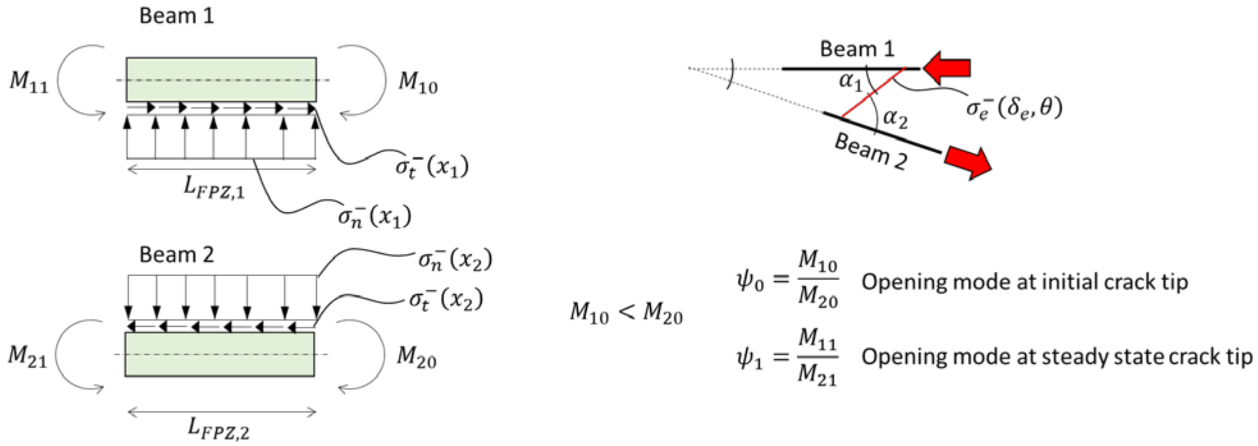

Figure 15. Tractions acting along the fracture process zone due to bridging fibres loaded in compression.

5.1.1. Bridging fibres in tension

By evaluating the relation between the two angles that a bridging fibre forms with the two surfaces it is anchored to, defined as α_1 and α_2 in Figure 14, the following conclusion can be drawn:

$$\left.\begin{aligned} \sigma_n^+(x_1) &= \sigma_e^+(\delta_e,\theta)\sin\alpha_1 \\ \sigma_t^+(x_1) &= \sigma_e^+(\delta_e,\theta)\cos\alpha_1 \\ \sigma_n^+(x_2) &= \sigma_e^+(\delta_e,\theta)\sin\alpha_2 \\ \sigma_t^+(x_2) &= \sigma_e^+(\delta_e,\theta)\cos\alpha_2 \end{aligned}\right\} \alpha_1 > \alpha_2 \Rightarrow \begin{aligned} \sigma_n^+(x_1) &> \sigma_n^+(x_2) \\ \sigma_t^+(x_1) &< \sigma_t^+(x_2) \end{aligned} \tag{5}$$

The moment contributions from the tractions in Figure 14 and Equation (5) can be defined as:

The DACOMAT project has received funding from the European Union's Horizon 2020 research and innovation program under GA No. 761072

$$\begin{array}{llll} \text{Moment contribution from} & \sigma_n^+(x_1) & \rightarrow & A_{n1}^+ \\ \text{Moment contribution from} & \sigma_t^+(x_1) & \rightarrow & A_{t1}^+ \\ \text{Moment contribution from} & \sigma_n^+(x_2) & \rightarrow & A_{n2}^+ \\ \text{Moment contribution from} & \sigma_t^+(x_2) & \rightarrow & A_{t2}^+ \end{array} \tag{6}$$

For the fibres loaded in tension (Figure 14) it is then possible to set up the following relation for the opening mode at the crack tip:

$$\psi_1^+ = \frac{M_{11}^+}{M_{21}^+} = \frac{M_{10} + A_{n1}^+ - A_{t1}^+}{M_{20} - A_{n2}^+ - A_{t2}^+} \tag{7}$$

where M_{10} and M_{20} are the moments acting on the two beam ends, and A_{ni}^+ and A_{ti}^+ are the moment contributions from the normal and tangential tractions, respectively, from a single bridging fibre loaded in tension. The relation between the moment contributions in Equation (7) gives an overview of how the relation between the moments in the two beams at a crack tip is affected by fibres loaded in tension. Since the moment contribution from the normal traction at the upper beam is positive and negative at the lower beam in Equation (7), their combined contribution will promote a shift towards mode II. The difference in magnitude of the tangential tractions, as defined in Equation (5), will also promote a shift towards mode II. This relation should hold for any fibre length as long as $\alpha_1 > \alpha_2$ in Figure 14.

5.1.2. Bridging fibres in compression

By evaluating the relation between the two angles that a bridging fibre forms with the two surfaces it is anchored to, defined as α_1 and α_2 in Figure 15, the following conclusion can be drawn:

$$\left.\begin{array}{l} \sigma_n^-(x_1) = \sigma_e^-(\delta_e, \theta)\sin\alpha_1 \\ \sigma_t^-(x_1) = \sigma_e^-(\delta_e, \theta)\cos\alpha_1 \\ \sigma_n^-(x_2) = \sigma_e^-(\delta_e, \theta)\sin\alpha_2 \\ \sigma_t^-(x_2) = \sigma_e^-(\delta_e, \theta)\cos\alpha_2 \end{array}\right\} \alpha_1 < \alpha_2 \Rightarrow \begin{array}{l} \sigma_n^-(x_1) < \sigma_n^-(x_2) \\ \sigma_t^-(x_1) > \sigma_t^-(x_2) \end{array} \tag{8}$$

The moment contributions from the tractions in Figure 15 and equation (8) can be defined as:

$$\begin{array}{llll} \text{Moment contribution from} & \sigma_n^-(x_1) & \rightarrow & A_{n1}^- \\ \text{Moment contribution from} & \sigma_t^-(x_1) & \rightarrow & A_{t1}^- \\ \text{Moment contribution from} & \sigma_n^-(x_2) & \rightarrow & A_{n2}^- \\ \text{Moment contribution from} & \sigma_t^-(x_2) & \rightarrow & A_{t2}^- \end{array} \tag{9}$$

For the fibre loaded in compression (Figure 15), it is then possible to set up the following relation for the opening mode at the crack tip:

$$\psi_1^- = \frac{M_{11}^-}{M_{21}^-} = \frac{M_{10} - A_{n1}^- - A_{t1}^-}{M_{20} + A_{n2}^- - A_{t2}^-} \tag{10}$$

where M_{10} and M_{20} are the moments acting on the two beam ends, and A_{ni}^- and A_{ti}^- are the moment contributions from the normal and tangential tractions, respectively, from a single bridging fibre loaded in compression. The relation between the moment contributions in Equation (10) gives an overview of how the relation between the moments in the two beams at the crack tip is affected by the fibres that are loaded in tension. Since the moment contribution from the normal traction at the upper beam is positive and negative at the lower beam in Equation (10), their combined contribution will promote a shift towards mode I. The difference in magnitude of the tangential tractions, as defined in Equation (8), will also promote a shift towards mode I. This relation should hold for any fibre length as long as $\alpha_1 < \alpha_2$ in Figure 15.

5.1.3. Combined effect of bridging fibres

The evaluation of Equations (5) and (7) indicate that bridging fibres loaded in tension will give the crack tip a mode shift towards mode II, whereas the evaluation of Equations (8) and (10) indicate that bridging fibres loaded in compression will give a mode shift towards mode I. The analysis presented above gave no information on the magnitude of the contributions. However, in the initial analysis performed on the survivability of single fibres described in DACOMAT deliverable 1.1 *Micromechanical modelling* (D1.1) [25], the fibres loaded in compression seem to fail by buckling at an early stage in the fracture process zone whilst the tension loaded fibres failed at significantly larger opening displacements. It is therefore assumed that the traction from bridging fibres loaded in tension is the larger contributor to the fracture resistance associated with fibre bridging. It follows that the crack tip will shift towards mode II as fibre bridging develops in the wake of the crack tip.

The assumptions that the illustration in Figure 6 are based upon no longer hold if the opening mode of the crack tip during initiation is not the same as for steady state delamination. The same goes for the transition from the R-curves in Figure 10 to those in Figure 12. The implications for the validity of Equation (4) needs further investigation.

A rising R-curve was assumed to be caused by fibre bridging directly. This assumed causality might not hold in light of the new finding. A shift in crack tip opening mode towards mode II will have a significant effect on the total fracture resistance as can be observed in Figure 11. Both fibre bridging and increased crack tip fracture resistance might therefore cause a rising R-curve. Increased crack tip fracture resistance is, however, a consequence of fibre bridging.

This new finding suggests that there could be a discrepancy between a fracture resistance calculated from the applied moments according to Equation (2) and calculated by integrating the cohesive tractions over the opening history of the crack end according to Equation (3). This will be examined in the next sub-section.

5.2. Optimisation procedure for determining a mixed mode cohesive law

In the previous section, it was shown that not every point along the FPZ experience the same opening history as experienced by the crack-end. The evolution of the crack-end may, therefore, not be representative for the R-curve evolution. In an ongoing study, the optimisation process for determining a mode I cohesive law [24] has been extended to a mixed mode cohesive law. The methodology was cumbersome, yet managed to produce mixed mode cohesive laws capable of predicting load-displacement behaviour of the same laminates subjected to standardised DCB and MMB testing. The cohesive laws were defined in the space of effective cohesive traction, effective opening displacement and opening mode angle. The cohesive law is illustrated in Figure 16 and listed in Table 1.

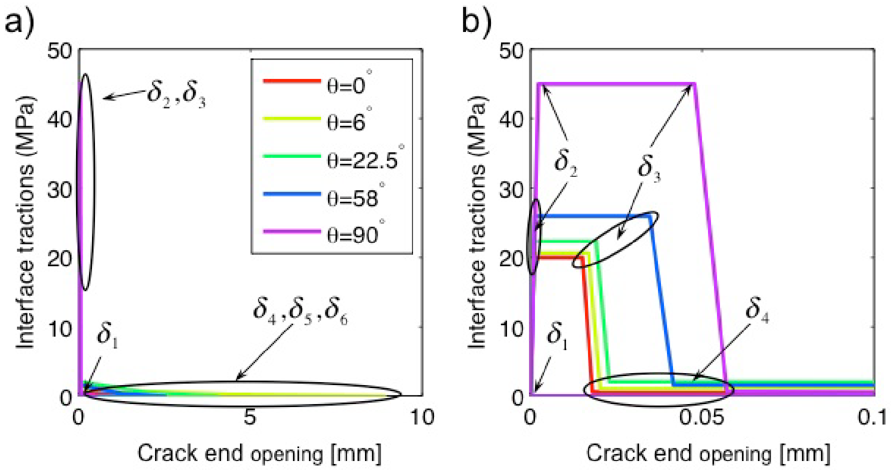

Figure 16. A mixed mode cohesive law defined for five different opening mode angles.

Table 1. The cohesive law is defined as a surface where the values are defined at specific locations and the linear interpolation between these.

	$\theta_1 = 0^\circ$		$\theta_2 = 6^\circ$		$\theta_3 = 22.5^\circ$		$\theta_4 = 58^\circ$		$\theta_5 = 90^\circ$	
l	$\delta_{e,l1}$ [mm]	$\sigma_{e,l1}$ [MPa]	$\delta_{e,l2}$ [mm]	$\sigma_{e,l2}$ [MPa]	$\delta_{e,l3}$ [mm]	$\sigma_{e,l3}$ [MPa]	$\delta_{e,l4}$ [mm]	$\sigma_{e,l4}$ [MPa]	$\delta_{e,l5}$ [mm]	$\sigma_{e,l5}$ [MPa]
1	0.0000	0.0000	0.0000	0.0000	0.0000	0.0000	0.0000	0.0000	0.0000	0.0000
2	0.0010	20.0000	0.0010	20.6155	0.0011	22.3082	0.0013	25.9500	0.0023	45.0000
3	0.0151	20.0000	0.0169	20.6155	0.0191	22.3082	0.0347	25.9500	0.0477	45.0000
4	0.0181	0.6200	0.0203	1.0660	0.0229	2.0816	0.0416	1.6089	0.0572	0.6975
5	1.5088	0.1568	4.4500	0.2696	2.0145	0.5264	1.2508	0.4069	0.2529	0.1764
6	3.0176	0.0000	8.9000	0.0000	4.0291	0.0000	2.5016	0.0000	0.5057	0.0000

The cohesive law was optimised to fit with the experimental results as shown in Figure 17. The initial reason for using an optimisation scheme to define the cohesive law was the skewedness in the observed opening displacements caused by anticlastic bending discussed in section 4.3. This method might have also fortuitously solved the challenge discussed in section 5.1. The blue curves in Figure 17 represent the R-curve produced by the FE analysis in which the cohesive law from Table 1 was used. If this response is representative for the FPZ-end behaviour, it should be possible to integrate the cohesive tractions along the opening histories of the FPZ-end for the FE simulations in Figure 17. The degree of mode mixity is here defined by M1/M2, so that mode I is -1 and mode II is 1. A value of zero represents one beam loaded with a bending moment and the other unloaded. The simulations with M1/M2 = 0.299 and 0.629 represents mixed mode delamination dominated by mode II.

The DACOMAT project has received funding from the European Union's Horizon 2020 research and innovation program under GA No. 761072

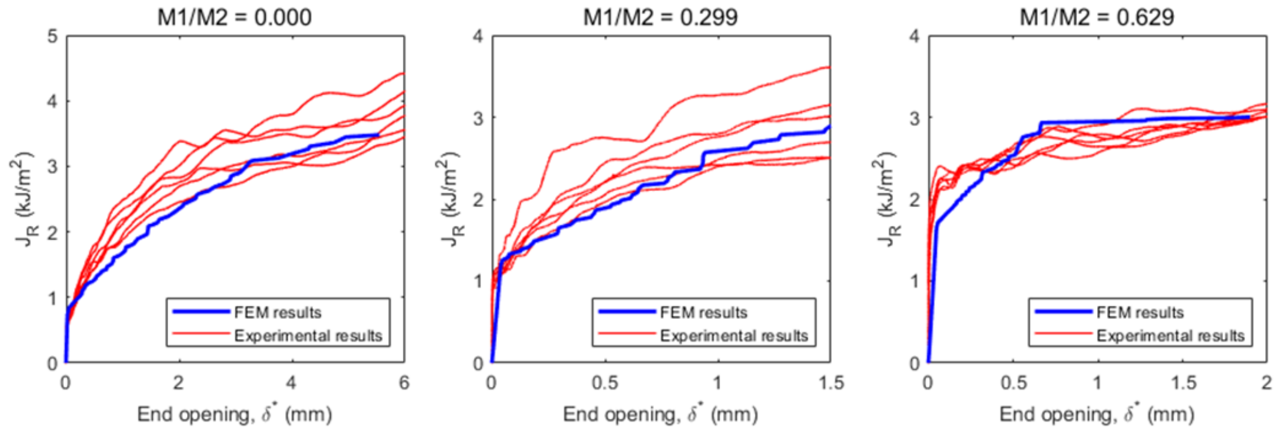

Figure 17. Experimental results and FE-simulations with optimised cohesive law.

The cohesive law listed in Table 1 represents a grid of known values. Any arbitrary value between these grid points needs to be interpolated from the known values in Table 1, as illustrated in Figure 18.

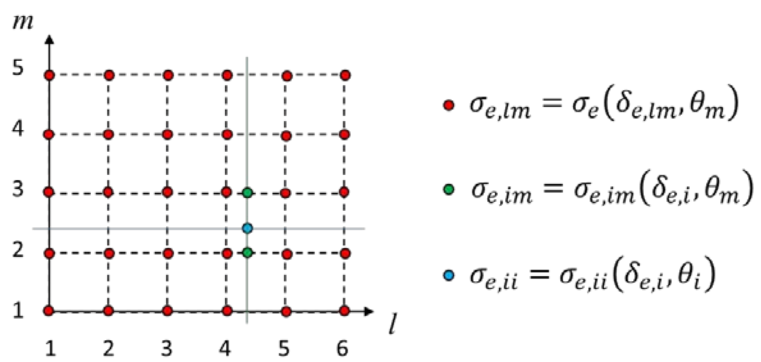

Figure 18. Interpolation scheme to define the value of an arbitrary position "ii" form the defined values at "lm", where "m" represent the steps in effective opening and "l" the steps in mode angle.

The interpolation is performed by first defining the value of $\sigma_{e,im}$ at *m*= m*:

$$\sigma_{e,im} = \left(\sigma_{e,l(m+1)} - \sigma_{e,lm}\right)\frac{\delta_i - \delta_{lm}}{\delta_{l(m+1)} - \delta_{lm}} + \sigma_{e,lm}. \tag{11}$$

Then the value of of $\sigma_{e,i(m+1)}$ is defined at *m* = m+1*:

$$\sigma_{e,i(m+1)} = \left(\sigma_{e,(l+1)(m+1)} - \sigma_{e,(l+1)m}\right)\frac{\delta_i - \delta_{(l+1)m}}{\delta_{(l+1)(m+1)} - \delta_{(l+1)m}} + \sigma_{e,(l+1)m}. \tag{12}$$

Finally, the value of $\sigma_{e,ii}$ at the arbitrary position "ii" is defined by interpolating the values of $\sigma_{e,im}$ and $\sigma_{e,i(m+1)}$ defined by equation (11) and (12), respectively:

$$\sigma_{e,ii} = \left(\sigma_{e,im} - \sigma_{e,i(m+1)}\right)\frac{\theta_i - \theta_m}{\theta_{m+1} - \theta_m} + \sigma_{e,im}. \tag{13}$$

The interpolation scheme finalised in equation (13) has to be done at every simulation step when integrating the cohesive tractions along the opening history of the crack end in accordance with:

$$J_{int}(\delta_{n,i+1},\delta_{t,i+1}) = \frac{1}{2}\begin{bmatrix}(\sigma_{n,ii}+\sigma_{n,(i+1)(i+1)})(\delta_{n,i+1}-\delta_{n,i})\\ +(\sigma_{t,ii}+\sigma_{t,(i+1)(i+1)})(\delta_{t,i+1}-\delta_{t,i})\end{bmatrix} + J_{int}(\delta_{n,i},\delta_{t,i}), \tag{14}$$

where,

$$\begin{aligned}\delta_{n,ii} &= \delta_{e,ii}\cos\theta_i\\ \delta_{t,ii} &= \delta_{e,ii}\sin\theta_i\\ \sigma_{n,ii} &= \sigma_{e,ii}\cos\theta_i\\ \sigma_{t,ii} &= \sigma_{e,ii}\sin\theta_i.\end{aligned} \tag{15}$$

The results from Equation (14) can be used to plot an R-curve for comparison with the blue curves plotted in Figure 17. This comparison is presented in Figure 19. The comparison can be seen as an evaluation of the assumption that Equation (3) is equivalent to Equation (2) in sub-section 4.2. The curves do not perfectly overlap as can be seen in Figure 19. The initial purpose of the optimisation procedure for determining the cohesive law was to circumvent the skewedness caused by the anticlastic bending effects discussed in section 4.3. The anticlastic bending effects should influence the initiation part of the R-curve and be dominant in mode I. It should not be present in pure mode II. Shifting from mode I to mode II should therefore reduce its effect. Furthermore, the effect should be insignificant for larger openings. The results presented in Figure 19 show that the discrepancy between the curves are not limited to small openings and does not decrease as the mode shifts towards mode II. It can be seen that the R-curves calculated from the applied moments have some oscillations. The same oscillations are not present in the red curves that are calculated from the cohesive law according to Equation (3). Both red and blue curves are here plotted from the same opening history. The beam ends in the analysis were given prescribed rotations. The moments used to calculate the blue R-curves are reaction forces recorded from location of the prescribed rotations.

The DACOMAT project has received funding from the European Union's Horizon 2020 research and innovation program under GA No. 761072

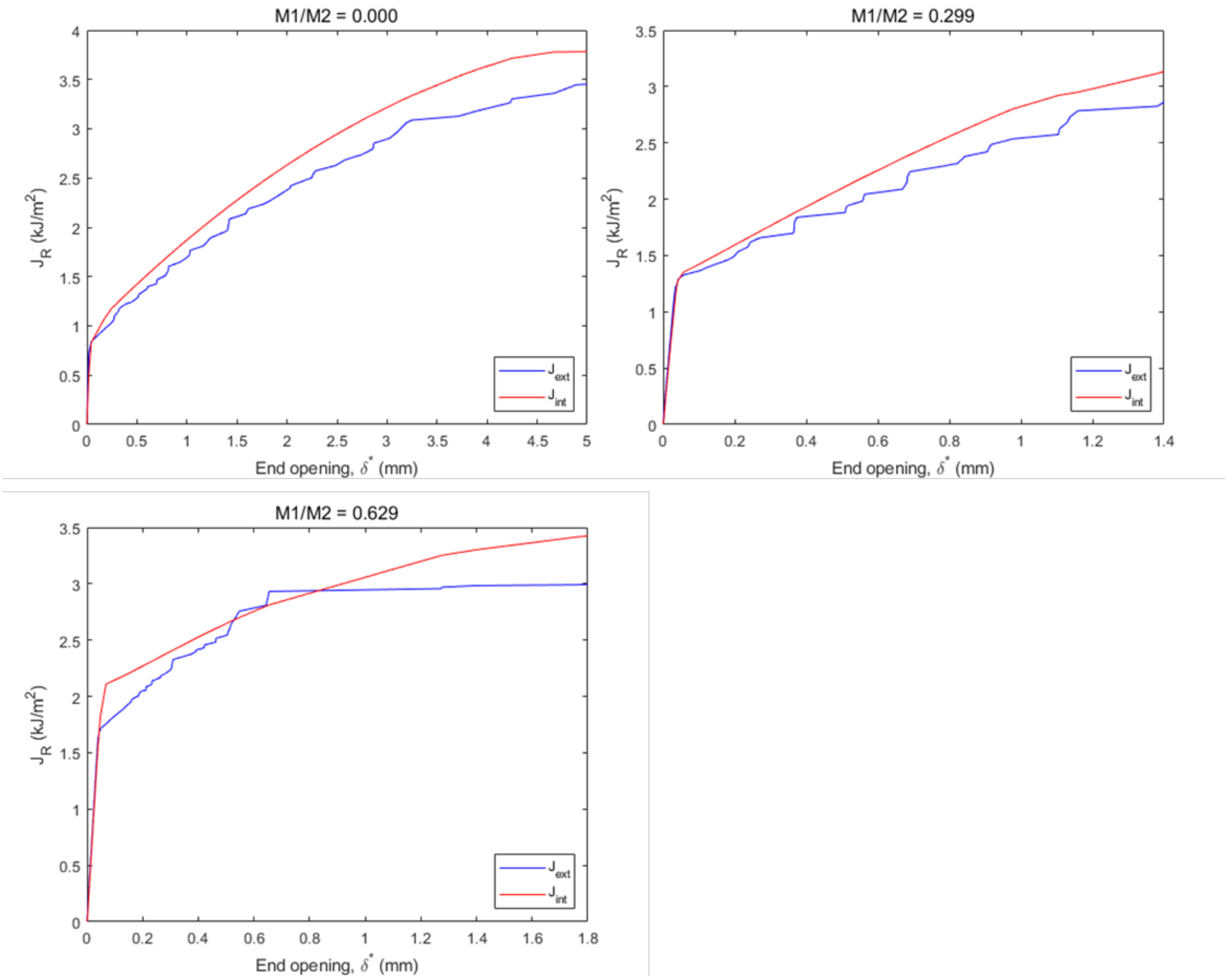

Figure 19. A comparison between equation (2) and (3) with data recorded from FE-simulations of three different mode mixities.

The DACOMAT project has received funding from the European Union's Horizon 2020 research and innovation program under GA No. 761072

6. Conclusions and recommendations for further work

The optimisation procedure described by Joki et. al. [24] seems to have inadvertently circumvented the unforeseen challenges discussed in this report. Of practical importance remains the need to refine and streamline the implementation of the optimisation procedure by improving the description of the cohesive law. Defining the cohesive law as a grid of values seems awkward and requires several restrictions on the optimisation procedure to reduce computational cost. It would be much more favourable to have the cohesive law based on a function defined by as few parameters as possible.

The functions describing the fibre bridging can be based on exponential decay functions by distinguishing between crack tip and fibre bridging. The crack tip could have simple bilinear or trapezoid shapes with limitations on critical tractions and the only optimisation variable could be total area under the curve. The two distinct laws could be included in a single cohesive element or included as two separate elements working in parallel at a given location.

The idea that the R-curve can be viewed as a potential function could be questioned by the findings presented in this report. If the R-curve is a potential function the fracture resistance at a given opening displacement should not depend on the opening history. The conclusions from sub-section 5.1 imply that a crack tip developed during steady state fracture resistance could dissipate a different amount of fracture energy on its way to full separation as that of the crack end, even though they both reach the same magnitude of opening displacement and mode angle at full separation. One way of handling this could be to view the R-curve, not as one single potential function, but rather as the sum of two decoupled potential functions, one for the crack tip and one for fibre bridging. Developing cohesive models that incorporate such a distinction should be straightforward and would demand an iterative characterisation process like the one discussed herein [24].

The parameter studies made available through the micromechanical model described in DACOMAT deliverable 1.1 *Micromechanical modelling* [25] will be very beneficial in the process of determining suitable functions that can be optimised for the fibre bridging law.

Finally, it would be beneficial for the continuing work on the characterisation of cohesive laws if experiments on DCB samples could investigate and compare different opening histories.

References

[1] P. Geubelle og J. Baylor, «Impact-induced delamination of composites: a 2D simulation,» *Composites Part B: Engineering,* pp. 589-602, 29 (5) 1998.

[2] B. Sørensen og P. Kirkegaard, «Determination of mixed mode cohesive laws,» *Engineering Fracture Mechanics,* pp. 2642-61, 43 (17) 2006.

[3] B. Sørensen og T. Jacobsen, «Determination of cohesive laws by the J integral approach,» *Engineering Fracture Mechanics,* pp. 1848-58, 70 (14) 2003.

[4] B. Sørensen og T. Jacobsen, «Characterizing delamination of fibre composites by mixed mode cohesive laws,» *Composites Science and Technology,* pp. 445-56, 69 2009.

[5] P. Olsson og U. Stigh, «ON THE DETERMINATION OF THE CONSTITUTIVE PROPERTIES OF THIN INTERPHASE LAYERS - AN EXACT INVERSE SOLUTION,» *International Journal of Fracture,* pp. R71-R76, 41 1989.

[6] L. Iannucci, «Dynamic delamination modelling using interface elements,» *Computers & Structures,* pp. 1029-48, 84 (15-16) 2006.

[7] V. Dantuluri, S. Maiti, P. Geubelle, R. Patel og H. Kilic, «Cohesive modeling of delamination in Z-pin reinforced composite laminates,» *Composites Science and Technology,* pp. 616-31, 67 (3-4) 2007.

[8] D. Xie, A. Salvi, C. Sun, A. Waas og A. Caliskan, «Discrete Cohesive Zone Model to Simulate Static Fracture in 2D Triaxially Braided Carbon Fiber Composites,» *Journal of Composite Materials,* 2025-46 (22) 2006.

[9] L. Bouhala, A. Makradi, S. Belouettar, A. Younes og S. Natarajan, «An XFEM/CZM based inverse method for identification of composite failure parameters,» *Computers & Structures,* pp. (91-7), 153 2015.

[10] P. Camanho, C. Davila og M. de Moura, «Numerical Simulation of Mixed-Mode Progressive Delamination in Composite Materials,» *Journal of Composite Materials,* pp. 1415-38, 37 (16) 2003.

[11] V. Tvergaard, «Effect of fibre debonding in a whisker-reinforced metal,» *Materials Science and Engineering: A,* pp. 203-13, 125 (2) 1990.

[12] S. El-Sayed og S. Sridharan, «Cohesive layer models for predicting delamination growth and crack kinking in sandwich structures,» *International Journal of Fracture,* pp. 63-84, 117 (1) 2002.

[13] B. Blackman, H. Hadavinia, A. Kinloch og J. Williams, «The use of a cohesive zone model to study the fracture of fibre composites and adhesively-bonded joints,» *International Journal of Fracture,* pp. 25-46, 119 (1) 2003.

[14] X. Xu og A. Needleman, «Void nucleation by inclusion debonding in a crystal matrix,» *Modelling and Simulation in Materials Science and Engineering,* pp. 111-32, 1 (2) 1992.

[15] M. van den Bosch, P. Schreurs og M. Geers, «An improved description of the exponential Xu and Needleman cohesive zone law for mixed-mode decohesion,» *Engineering Fracture Mechanics,* pp. 25-46, 119 (9) 2006.

[16] W. Wagner og C. Balzani, «Simulation of delamination in stringer stiffened fiber-reinforced composite shells,» *Computers & Structures,* pp. 930-9, 86 (9) 2008.

[17] V. Tvergaard og J. Hutchinson, «The relation between crack growth resistance and fracture process parameters in elastic-plastic solids,» *Journal of the Mechanics and Physics of Solids,* pp. 1377-97, 40 (6) 1992.

[18] Q. Yang og B. Cox, «Cohesive models for damage evolution in laminated composites,» *International Journal of Fracture,* pp. 107-37, 133 (2) 2005.

[19] R. Østergaard, «Buckling driven debonding in sandwich columns,» *International Journal of Solids and Structures,* pp. 1264-82, 45 (5) 2008.

[20] J. Rice, «A Path Independent Integral and the Approximate Analysis of Strain Concentration by Notches and Cracks,» *Journal of Applied Mechanics,* pp. 379-86, 35 (2) 1968.

[21] V. Li og R. Ward, «A novel testing technique for post-peak tensile behaviour of cementitious materials,» i *Fracture toughness and fracture energy – testing methods for concrete and rocks*, H. Mihashi, H. Takahashi og F. Wittmann, Red., Rotterdam, A.A. Balkema Publisher, 1989, pp. 183-195.

[22] P. P. .. 1. Anthony J og 38(1):R19-R21., «Instantaneous evaluation of J and C,» *International Journal of Fracture,* pp. R19-R21, 38 (1) 1988.

[23] G. Bao, S. Ho, Z. Suo og B. Fan, «The role of material orthotropy in fracture specimens for composites,» *International Journal of Solids and Structures,* pp. 1105-16, 29 (9) 1992.

[24] R. Joki, F. Grytten, B. Hayman og B. Sørensen, «Determination of a cohesive law for delamination modelling – Accounting for variation in crack opening and stress state across the test specimen width,» *Composites Science and Technology,* pp. 49-57, 128 2016.

[25] F. Grytten, «D1.1 Micromechanical modelling,» Dacomat, 2019.

The DACOMAT project has received funding from the European Union's Horizon 2020 research and innovation program under GA No. 761072